



SCIENTIA
IRANICA

Sharif University of Technology
Scientia Iranica
Transactions B: Mechanical Engineering
<http://scientiairanica.sharif.edu>



Numerical simulations of the hydrodynamic performance of the propeller with wake equalizing duct behind the ship

S. Rezaei^a, M. Bamdadinejad^{b,*}, and H. Ghassemi^b

a. *Department of Mechanical Engineering, Sharif University of Technology, Tehran, Iran.*

b. *Department of Maritime Engineering, Amirkabir University of Technology, Tehran, Iran.*

Received 28 May 2021; received in revised form 16 February 2022; accepted 27 June 2022

KEYWORDS

DTMB4119 propeller;
 KRISO Container
 Ship (KCS);
 Pre-swirl stator;
 Symmetric and
 asymmetric ducts;
 Propeller
 performance;
 Wake equalizing duct.

Abstract. The equalizing wake flow into the propeller behind the ship is important from the hydrodynamic performance viewpoint. In this study, numerical simulations of the DTMB4119 propeller with two symmetric and asymmetric duct types behind the KRISO Container Ship (KCS) are performed using Computational Fluid Dynamics (CFD). In order to improve the wake equaling flow, a combined duct and stators' configurations are installed before the propeller in the stern of the ship and its hydrodynamic performance is studied using CFD. A duct with the NACA4415 section and two types of stator configurations are selected. The STAR-CCM+ software using the finite volume discretization method was used to solve the governing equations of the fluid flow. For simulating the turbulence model, the standard $k-\omega$ model was used and the solution method was validated in comparison with the available experimental data. Output parameters including thrust coefficient and torque coefficient in the open-water condition and behind the ship are presented and discussed. The propeller performance after mounting the asymmetric and symmetric ducts are improved by 4.8% and 6.57%, respectively. Therefore, it is concluded that the symmetric duct is more affected by the propeller performance and, hence, fuel consumption is reduced considerably.

© 2022 Sharif University of Technology. All rights reserved.

1. Introduction

Today, ship owners around the world are looking for solutions to three major challenges: diminishing costs, enhancing efficiency, and reducing impact on the environment. Several augmentation devices for energy saving can be considered. It should be noted that the applicability of such devices and technologies depends on ship type, ship size, operation profile, and other fac-

tors. Thus, decision-making for each device is required to go through the normal process of technical feasibility aspects and economic cost-effectiveness analysis for the specific ship under consideration.

One of the efficient devices functions via a combination of Wake Equalizing Duct (WED) and Pre-Swirl Stator (PSS), as shown in Figure 1. The stator blades create a pre-swirl, giving the propeller a more favorable angle of attack. The duct increases flow velocity towards the propeller and creates a forward-directed force with its wing-shape section. These features facilitate possible energy saving up to 8% for full-form slower ships, such as tankers and bulkers. The improvement of the propulsion efficiency of these types of ships will contribute largely to the reduction

*. *Corresponding author.*
E-mail address: miladbamdadi@aut.ac.ir (M. Bamdadinejad)



Figure 1. (a) Wake equalizing duct mounted on the ship's stern, (b) Asymmetric duct.

of polluting emissions and to the saving of fossil fuels in shipping [1]. According to the statistical studies on the fuel consumption of various vessels since the year 1980, even a 1% reduction in the fuel consumption of an oil tanker that consumes 60–100 tons/day (when moving) and imposes a daily cost of about \$35–50 thousand on the owner (increasing exponentially based on the voyage length/time) is very important [2]. Figure 1(a) shows a WED mounted on the ship's stern [3], and Figure 1(b) shows an asymmetric duct [4].

Generally, two approaches are employed to reduce engine power. One approach is to design an optimum hull that reduces the resistance, and the second approach is to improve the propulsion efficiency. To improve the thrust and efficiency, many types of Energy-Saving Devices (ESDs) are employed in three zones of the ship stern; see Chapter 13 of the referenced book authored by Carlton [5].

Many numerical and experimental works were carried out to analyze and design the ESD [6–11]. Anderson (1988) applied the VLM to obtain the hydrodynamic behavior of the propeller performance [12] using the Vortex Lattice Method (VLM) and defining a propeller blade surface replaced by the vortex distribution. Later, many researchers have worked more precisely on these methods and used the Boundary Element Method (BEM) separately to study the flow behavior in steady-state ducted propellers [13,14]. Baltazar et al. (2012) evaluated the torque and thrust of a ducted propeller in an open water mode using the panel method where the propeller hydrofoil is modeled as a well or spring. In this method, conditions considered as the problem default are closer to those governing the propeller performance in open water and the hull and wake effects on the propeller efficiency are studied [15]. Lee et al. (2016) employed a new structural safety assessment method for ESD. In this method, Morison equation was solved for a velocity at a certain probability level using two neural network methods as well as time domain simulation and Gamble fitting method [16]. Gaggero et al. (2018) evaluated propulsion efficiency improvements using Propeller Boss Cap Fin

(RBCF) device optimization and Computational Fluid Dynamics (CFD) analysis. In order to solve the RANS equations, parametric descriptions of RBCF properties and an optimization algorithm were applied in Open FOAM software. The results demonstrated that the efficiency of the model scale increased by about one percent, which could reach a significant amount of four percent in the unrefined propeller design [17]. Nowruzi and Najafi (2019) investigated the effects of three different pre-swirl ducts on the propulsion performance of a Series-60 ship by experimental and numerical methods [18]. Tacar et al. (2020) used CFD analysis and experiments of a new model with a larger model of a container ship to investigate the Gate Rudder system and the effect of Gate Rudder on ship performance [19]. Obwogi et al. (2021) studied the effect of rudder bulb diameter, thrust fin, span, chord length, and angle of attack on propulsion efficiency using CFD [20].

BEM and CFD simulation methods are widely used as important tools to improve the efficiency and performance of the propeller design. Ghassemi et al. published many types of research by numerical methods (BEM and CFD) to simulate the propeller performance with different configurations under different operating conditions [21–27].

WED is one of the most common ESDs used to improve the propulsion performance of a ship, propeller-excited vibrations, and viscous resistance forces. Many studies have been done on WED for the past three decades, most of which have attempted to increase propulsion efficiency [28]. A commercial code called “Comet” was developed by Ok and Hamburg-Harburg (2005) using the RANSE method to study the flow around a WED [29]. Korkut (2006) conducted a study on energy saving in powering characteristics of cargo ships using the concept of partial WED [30]. Celik (2007) explored the effect of WED on the propulsion performance of a chemical tanker using the RANS numerical method for various WED arrangements at different speeds of many ships [31]. Heinke and Hellwig-Rieck (2011) investigated the effect of the Reynolds number on the flow around the appendages and on

the propeller in a typical container ship by WED and vortex generator fins [32]. A model was developed to improve the performance of a PSS and was used to estimate power savings. In this study, the circulation distribution method was employed based on the characteristics of the propellers [33]. Using a numerically variable method, Lee et al. (2019) designed an asymmetric stator using an auxiliary function by displaying the lifting lines of a vortex propeller and a stator [34]. Han (2019) estimated the energy saving efficiency of a PSS using the numerical method based on the lifting-surface method as well as the RANS equations, and the viscous flow around the hull in three systems: propeller in open water, the towing resistance experiment, and the self-propulsion test [35]. In another study, the effect of angle-axis PSS was investigated using a suitable design method for each blade or location for the radius with respect to the hydrodynamic pitch angle in order to improve the propulsive efficiency in non-uniform flow fields of the stern [36]. Furcas et al. (2020) proposed a Simulation-Based Design Optimization method (SBDO) to design an ESD based on the concept of WED [37]. Nadery and Ghassemi (2020) carried out the hydrodynamic performance of the KP505 propeller behind the KRISO Container Ship (KCS) with and without PSS and duct. It was concluded that good design increased efficiency by 1.67% and a bad design might reduce efficiency by 3.25% [38]. Koushan et al. (2020) numerically and experimentally investigated the effect of a PSS on propulsion efficiency in both model-scale and full-scale modes [39]. Recently, Nadery et al. (2021) numerically evaluated the impact of four ESDs including PSS, WED, and Pre-Swirl Ducts called PSD-1 and PSD-2 to improve the propeller performance of the KCS container ship [40]. Another study examined the effect of a new PSS configuration connected to the KP505 propeller on the propulsion performance of the KCS container ship [41]. Su et al. (2021) performed numerical and experimental analyses on a 25-meter ore carrier model to investigate the operation of ESDs, including a PSS and a rudder bulb [42]. Guo et al. (2021) used a bulk carrier-scale model to study the flow mechanism of a ship and the working principles of energy-saving appendages [43]. Qin et al. (2021) numerically measured the flow effect of a pre-swirl pump jet propulsor based on improved delayed detached eddy simulation [44]. Mikkelsen et al. (2022) examined the nominal wake fields in five different heading conditions for the KCS container ship in regular waves with a wavelength equal to the length of the ship [45].

Following a detailed review of the literature, the most published works in this field revolve around the propeller KP505 and the KCS ship hull, which were investigated and presented by the third author of the present paper. However, this study provides a new propeller of DTMB4119 matching the KCS and

discusses how it works. The objective is to determine the hydrodynamic performance of this propeller by installing new duct and PSS, while no one worked on this special type of propeller.

To evaluate this propeller type and the proposed combination of the duct and PSS, two types of symmetric and asymmetric PSS including ducts at different velocities have been investigated. The hydrodynamic performance of the propeller (thrust and torque coefficients) under four cases (open-water, without duct, symmetric duct, and asymmetric duct) at different velocities are presented and discussed.

The remainder of the paper is organized as follows. Section 2 describes the governing equations and different turbulence models. Section 3 presents numerical implementation, computational domains, and boundary conditions. Section 4 presents and discusses the numerical results of the propeller performance under different upstream wake equalizing devices at various speeds. Finally, Section 5 draws the conclusions.

2. Governing equations

Here, the flow simulation and propeller modeling are the main concerns, and the fluid flow is studied in the control volume; therefore, a conversion tool that can provide its “general transfer theorem” is required. Governing equations use two basic hydrodynamic equations: conservation of mass (the continuity equation) and conservation of momentum (Navier-Stokes equations).

2.1. Continuity equation for the turbulent flow

In its general form, the continuity equation is expressed as follows:

$$\frac{\partial \rho}{\partial t} + \text{div}(\rho U) = 0, \quad (1)$$

where ρ and U are the density and velocity vectors of the fluid, respectively. This equation is valid for the instantaneous values of the turbulent flow. The temporal averaging of Eq. (1), replacing momentary quantities with average temporal values plus the fluctuating values, and using Reynolds averaging rules will yield Eq. (2) as follows:

$$\frac{\partial \bar{\rho}}{\partial t} + \frac{\partial}{\partial x_i} (\bar{\rho} \bar{u}_i) + \frac{\partial}{\partial x_i} (\overline{\rho' u'_i}) = 0, \quad (2)$$

where $\bar{\rho}$ and $\bar{\rho}'$ are the average density and the average oscillation density; and \bar{u}_i and \bar{u}'_i are the average velocity and the average oscillating velocity, respectively. For an incompressible flow, since $\rho' = 0$, Eq. (2) will be as follows:

$$\frac{\partial \bar{u}_i}{\partial x_i} = 0. \quad (3)$$

2.2. Momentum equation for the turbulent flow

Momentum equations for an incompressible viscous flow are as follows:

$$\rho \left(\frac{\partial u_i}{\partial t} + u_j \frac{\partial u_i}{\partial x_j} \right) = B_i - \frac{\partial P}{\partial x_i} + \mu \frac{\partial^2 u_i}{\partial x_i \partial x_j}, \quad (4)$$

where B_i , P , and μ are the body force, fluid hydrostatic pressure, and fluid viscosity, respectively. This equation is valid for both steady and turbulent flows; in the latter, dependent variables (velocity, pressure, etc.) are all time dependent. Expressing Eq. (4) in terms of average temporal quantities, i.e., placing $u_i = u'_i + \bar{u}_i$ and $P_i = P'_i + \bar{P}_i$ (u_i , u'_i , and \bar{u}_i are called instantaneous velocity, oscillating velocity, and average velocity and P_i , P'_i , and \bar{P}_i are called instantaneous hydrostatic pressure, oscillating hydrostatic pressure, and average hydrostatic pressure, respectively) in Eq. (4), and simplifying and re-applying the temporal averaging will yield Eq. (5) as follows:

$$\rho \left(\frac{\partial \bar{u}_i}{\partial t} + \bar{u}_j \frac{\partial \bar{u}_i}{\partial x_j} + \overline{u'_j \frac{\partial u'_i}{\partial x_j}} \right) = \bar{B}_i - \frac{\partial \bar{P}_i}{\partial x_i} + \mu \frac{\partial^2 \bar{u}_i}{\partial x_i \partial x_j}, \quad (5)$$

where \bar{B}_i and \bar{P}_i are average body force and average fluid hydrostatic pressure, respectively. Term three on the left side is usually expressed differently. Since $\frac{\partial u'_j}{\partial x_j} = 0$ is a continuity equation of incompressible flows, adding and subtracting $u'_j \frac{\partial u'_i}{\partial x_j}$ to and from the sides of Eq. (5) will result in the turbulent flow momentum equation as follows:

$$\rho \left(\frac{\partial \bar{u}_i}{\partial t} + \bar{u}_j \frac{\partial \bar{u}_i}{\partial x_j} \right) = \bar{B}_i - \frac{\partial \bar{P}_i}{\partial x_i} + \frac{\partial}{\partial x_i} \left(\mu \frac{\partial \bar{u}_i}{\partial x_j} \overline{\rho u'_i u'_j} \right). \quad (6)$$

The only difference between Eq. (6) and momentum equation with instantaneous quantities lies in the addition of the last term, i.e., $\overline{\rho u'_i u'_j}$, which is idiomatically called the turbulence tension or Reynolds's tension.

2.3. Standard $k - \varepsilon$ model

Due to its simplicity in understanding and programming, this model is very popular. It is used in the Boussinesq relationship and expresses the turbulent field using two variables: the turbulent kinetic energy (k) (Eq. (7)) and the rate of dissipation of turbulent kinetic energy (ε) (Eq. (8)):

$$k = \frac{1}{2} \overline{u'_i u'_i}, \quad (7)$$

$$\varepsilon = \left(\frac{\mu}{\rho} \right) \overline{u'_{i,j} u'_{i,j}}. \quad (8)$$

Dimensional analyses have shown that the turbulent viscosity is directly proportional to the velocity and

the scale length of large vortices in the turbulent flow field. Thus, we have:

$$\mu_t = C_\mu \rho \frac{k^2}{\varepsilon}, \quad (9)$$

where μ_t is called turbulent viscosity and C_μ is equal to 0.09. ε and k are found by semi-experimental Eqs. (10) and (11). In the following relation, σ_ε is the turbulent Schmidt number and equal to 1.3, σ_k is the Prandtl number and equal to 1, G (shear production term) is the turbulence kinetic energy produced by the average flow-turbulent flow field interaction, and B is the production-buoyancy loss due to the flow fluctuating density field. C_1 , C_2 , and C_3 are called model constants, which are 1.44, 1.92, and -0.33 , respectively.

$$\rho \frac{\partial k}{\partial t} + \rho u_j k_j = \left(\mu + \frac{\mu_t}{\sigma_k} k_j \right)_j + G + B - \rho \varepsilon, \quad (10)$$

$$\begin{aligned} \rho \frac{\partial \varepsilon}{\partial t} + \rho u_j \varepsilon_j &= \left(\mu + \frac{\mu_t}{\sigma_\varepsilon} \varepsilon_j \right)_j + C_1 \frac{\varepsilon}{k} G \\ &+ C_1 (1 - C_3) \frac{\varepsilon}{k} B - C_2 \rho \frac{\varepsilon^2}{k}. \end{aligned} \quad (11)$$

2.4. $k - \omega$ SST model

The SST is, in fact, an optimized $k - \omega$ standard model, which is itself a modified form of the Wilcox model at low Reynolds, compressibility, and shear flow dispersion effects. To use both $k - \omega$ and $k - \varepsilon$ equations, an integration function is introduced which equals 1 in areas near the wall (to activate $k - \omega$ model) and zero in those far from the wall (to activate $k - \varepsilon$ model); here, a negative point is the possibility of instability and poor convergence due to model-to-model switching.

$$\begin{aligned} \frac{\partial(\rho k)}{\partial t} + \frac{\partial}{\partial x_j} (\rho U_j k) &= \frac{\partial}{\partial x_j} \left[\left(\mu + \frac{\mu_t}{\sigma_k} \right) \frac{\partial k}{\partial x_j} \right] \\ &+ P_k - \beta' \rho k \omega + P_{kb}, \end{aligned} \quad (12)$$

$$\begin{aligned} \frac{\partial(\rho \omega)}{\partial t} + \frac{\partial}{\partial x_j} (\rho U_j \omega) &= \frac{\partial}{\partial x_j} \left[\left(\mu + \frac{\mu_t}{\sigma_\omega} \right) \frac{\partial \omega}{\partial x_j} \right] \\ &+ \alpha \frac{\omega}{k} P_k - \beta \rho \omega^2 + P_{\omega b}. \end{aligned} \quad (13)$$

In Eqs. (12) and (13), U is the velocity vector, ρ the density, and P_k the turbulence production rate. Table 1 provides a list of the constants used in the equations.

Table 1. The stability used in the turbulence model.

α	β	β'	σ_k	σ_ω
5.9	0.075	0.09	2	2

3. Numerical implementation

In the CFD, the meshing of the computational domain is of great importance. It seems that more than 50% of the entire endeavor is dedicated to defining geometry and meshing production. CFD is known as an important tool for the design of industrial products and processes related to fluids engineering because the development of strong hardware in the 1990s led to a considerable growth in this field and the numerical method entered the computation field on a larger scale.

In numerical solutions, different methods namely the Finite Difference Method (FDM), Finite Volume Method (FVM), Finite Element Method (FEM), and BEM are used to solve the equations. Since this study uses the FVM, it is described here with its solution algorithm which involves the following four steps:

- Integrating the equations governing the fluid flow on the control volume;
- Discretizing and converting the integral equations into a set of algebraic equations;
- Selecting the solution method of the basic equations governing the flow (Navier-Stokes and continuity equations);
- Solving the set of algebraic equations.

The STAR-CCM+ software was used to numerically simulate all parts of this study. Since the flows around the ship had high Reynolds numbers, the turbulent flow method was selected using the $k - \epsilon$ turbulence model for ship modeling. The y^+ values were evaluated and selected based on the turbulence model. Free surface boundaries were calculated using the Volume Of Fluid (VOF) method. Also, the standard $k - \epsilon$ turbulence model and numerical method of the rotating flow of the propeller Multiple Reference Frame (MRF) were used for propeller modeling. Here, the next steps are:

- Generating a problem geometry;
- Creating a solution domain, producing a mesh or discretizing the domain;
- Explaining software settings for simulation purposes;
- Describing the general trend of the problem solution.

3.1. Test case: Model of ship hull and propeller

3.1.1. DTMB4119 propeller

To calculate the propeller hydrodynamic performance from either an empirical or theoretical standpoint, it is essential to have a detailed understanding of propeller geometry and the corresponding definitions used. Depending on the type of analysis and the

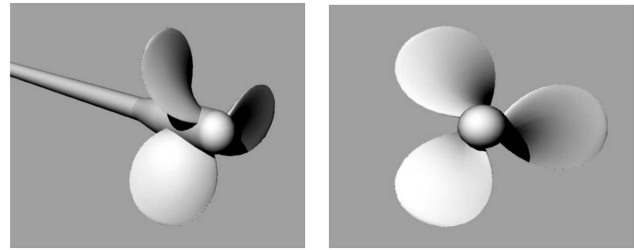


Figure 2. Different view of DTMB4119 propeller.

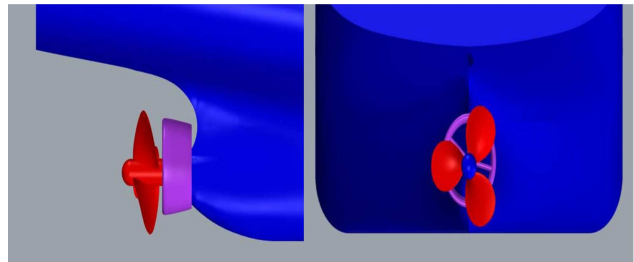


Figure 3. Propeller with the duct in the stern.

modeling sensitivity, it is quite necessary to design carefully and pay attention to the geometry structure of the propeller under consideration. This research used the DTMB4119 propeller comprising three blades. Due to its high accuracy and capability, the Rhino software was used to generate the propeller geometry and make a smooth and fair surface. Figure 2 shows different views of the propeller being studied and Table 2 lists its specifications. In addition, the propeller with the designed duct on the stern of the ship is shown in Figure 3.

3.1.2. The KRISO Container Ship (KCS)

The KCS is a modern container ship with a bulbous bow used to explore conceptual data inflow physics as well as validate CFD models [46,47]. The KCS container ship model was used to evaluate the propeller performance in the wake field. Figure 4 and Table 3 show the geometry and features of the model under study; the main ship was scaled by 0.03165 coefficient. DTMB4119 and KP505 as two standard marine propellers are used for the validation of numerical modeling in several types of research, although the KP505 is defined as the original propeller used for KCS

Table 2. Principal parameters of DTMB4119 propeller.

Propeller diameter (m)	0.3048
Expanded Area Ratio (EAR)	0.607
Number of blades	3
Pitch ratio	Variable
Rake (deg)	0
Skew (deg)	0
Blade section	NACA66 $a = 0.8$
Rotation direction	Right

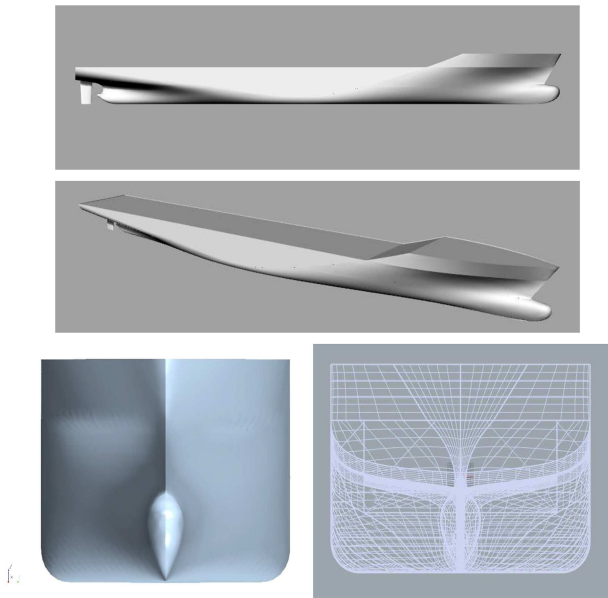


Figure 4. Different view of the KCS model.

Table 3. Principal parameters of the KCS model.

Hull parameter	Value
Length between perpendicular, LPP (m)	7.2786
Length of Water Line, LWL (m)	7.357
Breadth, B (m)	1.019
Depth, D (m)	0.6013
Draft, T (m)	0.3418
Wetted area surface (m^2)	9.4379
Midship section coef. [-]	0.9849
Block coef. [-]	0.6505

and modeling the wake pattern DTMB4119 was not applied to KCS hull. Thus, an attempt is made here to examine its performance for KCS in our research as an innovative act.

3.2. Computational domain

3.2.1. Computational domain of the ship model

To ensure a viable problem-solving capability and high accuracy and to simulate the flow around the ship model, the STAR-CCM+ software was selected for the present calculations. Considering the studies done on the modeling of the ship motion, a rectangular cube was selected for the computational domain where the ship motion simulation was performed, instead of moving the ship, based on the assumption that water flowed from one side of the domain as the input and hit the ship front. This is, in fact, a simulation method of the ship motion without using highly altered meshing that speeds up the process and reduces the computational cost while maintaining accuracy. The ship is a 2DOF object defined in the heave and pitch directions and is modeled using a two-phase model. Since the ship structure is symmetrical, only half of it was simulated. Figure 5 shows the computational domain dimensions and plan in terms of the ship length.

3.2.2. Computational domain of the propeller model

Here, two types of domains for the propeller simulation were used, i.e., cubical and cylindrical, with equal distances (Figures 6 and 7). After checking the numerical results with experimental data, the cubical domain was selected due to fewer errors (see Section 4). In simulations, domains are both fixed and rotating and modeling of the rotational motion of the propeller is done by the rotating disk (rotating cylinder) method; in addition, that of the water flow is based on the fixed domain which involves the rotating domain.

3.3. Meshing of the computational domain

Many encountered problems in the real world involve complex geometries for which creating a structured block mesh of hexagonal or quadrilateral cells is time-intensive. However, the computational time and, hence, the cost can be reduced using unstructured meshes with triangular-quadrilateral cells; if the geom-

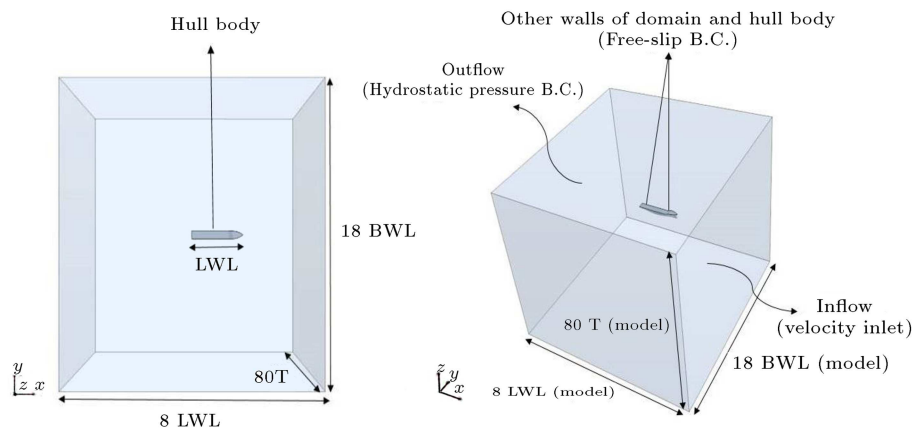


Figure 5. Schematic of the computational domain and boundary conditions of the ship.

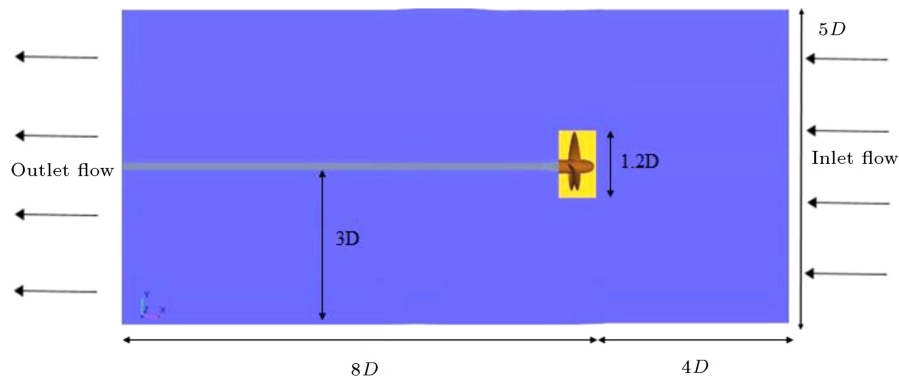


Figure 6. Rectangular cubic computational domain and boundary conditions of the propeller with the rotating domain.

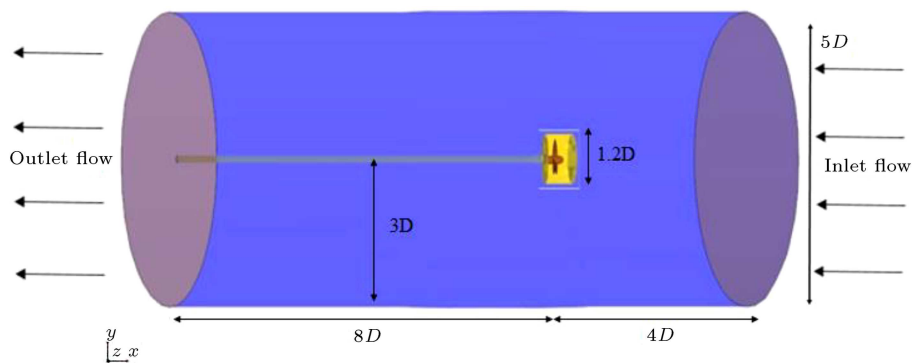


Figure 7. Cylindrical computational domain and boundary conditions of the propeller with the rotating domain.

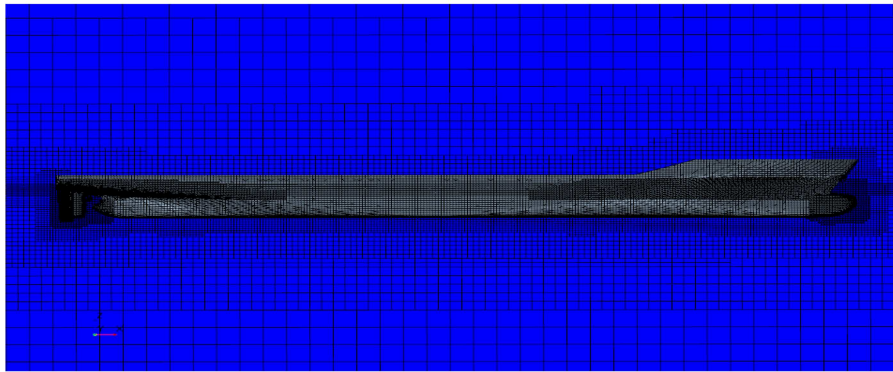


Figure 8. The meshing of the computational domain.

entry is simple, both ideas will take equal time. Another point worth noting in meshing and modeling is that the mesh and flow regime should match each other. Since convergence takes place better and faster for hexagonal-quadrilateral meshes, a great deal of effort was made for all areas to be created with these meshes to save both solution time and cost and reach more accurate solutions in the end.

Here, the emphasis is on the free water surface meshing because of the ship's two-phase computational domain. To increase the computational accuracy in the front and rear parts of the ship greatly affecting the output results, a separate control volume was established to make meshes finer. The hull periphery

Table 4. Specifications of the boundary layer.

Number of layers	12 layers
First layer thickness	0.1 mm
The overall thickness of the boundary layer	3 mm

meshes should be small enough to sense the effects of the free surface. Therefore, about 6,000,000 meshes were used for meshing the ship hull. Specifications of the important hull boundary layer are listed in Table 4, and the computational domain meshing is shown in Figure 8.

Since the propeller is fully submerged and not considered as a free surface, the computational domain

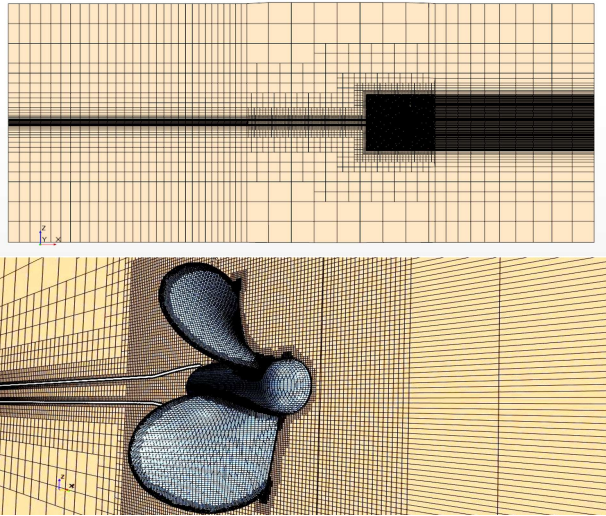


Figure 9. Computerization of the propeller's computational domain.

is considered in a single phase. To increase the accuracy, finer meshes were used in the rotating cylindrical sub-domain where it is close to the propeller blades, and to reduce the computational costs, meshes used far from the propeller were relatively larger (Figure 9).

Upon applying meshing and wall functions, the first node distance from the wall surface called y^+ should be considered. If the latter is too large, the first node may lie beyond the boundary layer, causing the functions to be applied too far from the wall, and if it is too small, this node will lie in the steady zone of the boundary layer where the related functions are invalid. The first wall thickness of the boundary layer (Δy) can be obtained through the approximation of Eq. (14) as follows:

$$\Delta y = \sqrt{74} L y^+ \text{Re}_L^{-13/14}, \quad (14)$$

where L is the ship length and Re_L is the Reynolds number based on the ship's length.

However, the use of wall functions will reduce the separation estimation and accuracy in vortex flows. To use the SST and $k-\omega$ turbulence models, we should have $y^+ < 300$, and to benefit from low-value Reynolds models, $y^+ < 2$ is required which is not quite easy due to the massive computational volume in most industrial applications. Figures 10 and 11 show the contour y^+ on the propeller and the ship hull, respectively. Table 5 shows the comparison of the calculated resistance coefficient (C_t) of the bare hull with the experimental value at a speed of 2.196 m/s ($Fn = 0.26$). This speed is the service speed for the KCS which takes 24 knots. It can be seen that there is close agreement between the calculated and experimental values and the corresponding relative error is about 4%.

3.4. Computational settings

Specifications of the ship, propeller, domain, solver

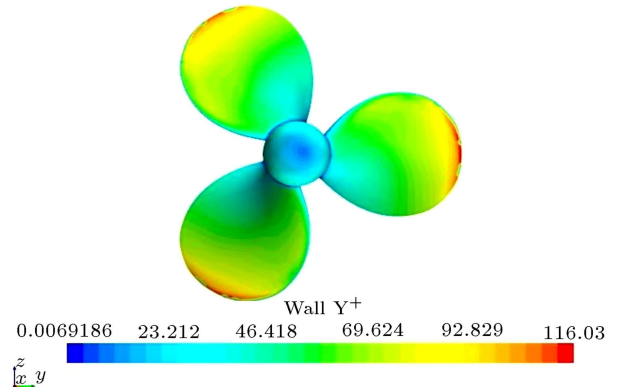


Figure 10. The y^+ contour on the propeller.

Table 5. Comparison of resistance coefficient at the model speed of $V_M = 2.196$ m/s ($Fn = 0.26$).

Resistance coef.	Calculated	Exp.	Error (%)
$10^3 C_t$	3.415	3.554	4.1%

Table 6. Numerical characteristics used in the software.

Characteristics	Propeller modeling	Ship modeling
The solver	Open water	Behind the ship
Time step	0.0005	0.04
Number of loops in each time step	—	10
Turbulent model	$k-\omega$ SST	$k-\varepsilon$

conditions, subdomains, boundary conditions, and so on are the issues that require specific techniques to be determined in the software setting. Setting boundary conditions that can accurately reflect the real conditions is important in acquiring accurate results. Boundary conditions are a set of features and conditions that need to be fully defined on the boundaries of the solution domain so that the flow is simulated. In the solver section, the maximum iterations are determined for solving the governing equations in each time step and the remaining is used to control the solution of the equations. The number of iterations and the acceptable remainder are important factors in the solution time. To simulate the ship motion, the unsteady method is employed to work out a solution, and in the case of the propeller, the steady method is adopted. Table 6 shows the characteristics of the applied numerical model.

3.5. Meshes of the solution strategy

The general simulation process and modeling strategy are shown in Figure 12. The simulation takes five general steps to complete:

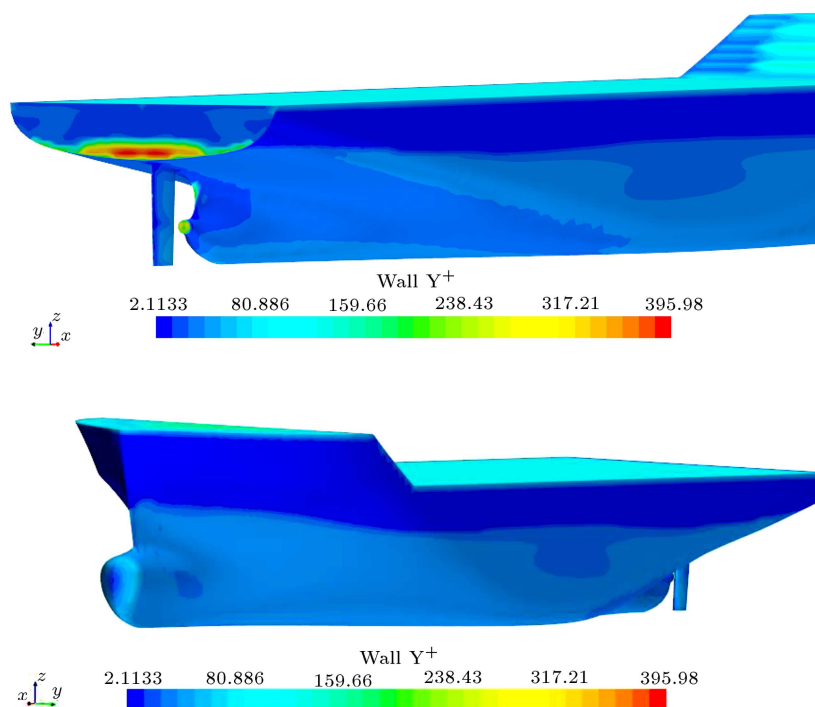


Figure 11. The y^+ contour on the ship hull.

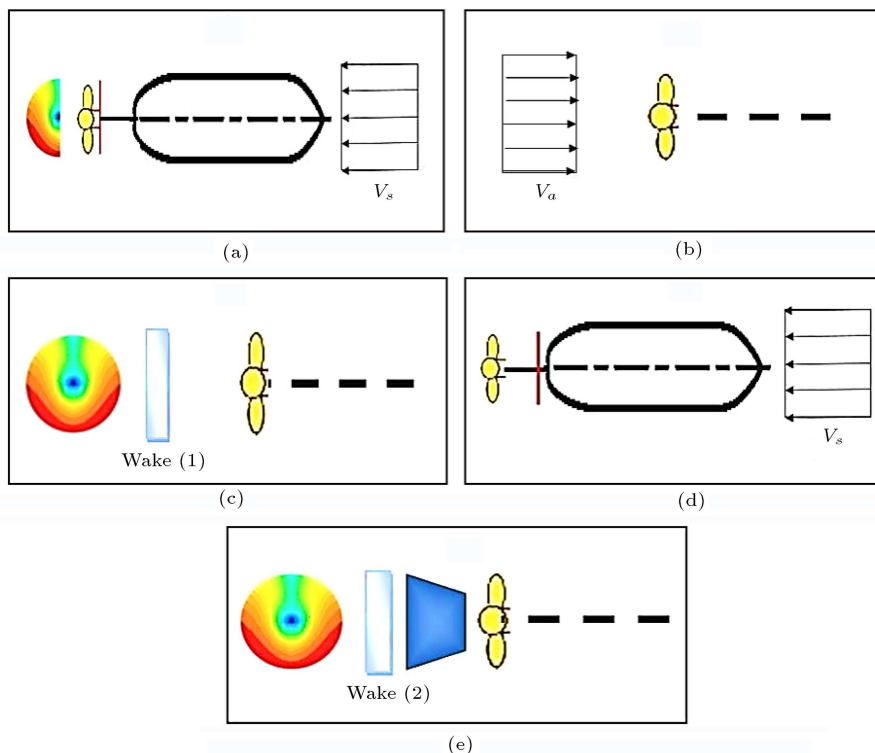


Figure 12. The general simulation process and modeling strategy.

(a) **Modeling the ship.** In this case, upon initiating the software and defining the ship geometry, a square box was plotted as the solution domain. Since the ship hull was symmetrical, half of it was simulated to speed up the calculations and

the problem was solved by defining the center of gravity and ship velocity and setting the meshes and time steps. To obtain the problem outputs, a circular plate was defined and the flow velocity results were recorded on it;

- (b) **Modeling the propeller in open water conditions.** In this case, mesh settings were performed for the steady solution after defining the propeller geometry in the software and determining the solution domain (input, output, and wall). The thrust and torque coefficients and the efficiency (according to the last recorded results) were extracted following the convergence of the solution results;
- (c) **Modeling the propeller behind the ship.** In this case, besides observing the solution and geometry conditions, the data recorded on the circular plate were added to the simulation as the input (input flow) and in doing so, the effect of the ship hull axial wake was considered in the propeller performance. The recorded input in this step is saved to an Excel file. The data include the velocity components (i, j, k) at a known local point;
- (d) **Wake measurement before duct installation location.** In this step, the hull wake is measured again and stored before the point intended for the duct installation;
- (e) **Modeling the symmetrical and asymmetrical duct sections behind the propeller.** The duct is designed in the Rhino software based on the wake model recorded in step (b) and placed in the front part of the propeller. The problem is then solved to extract the thrust and torque coefficients (Figure 12).

4. Results and discussion

Before presenting and analyzing the results obtained from the numerical solution of the flow on the selected ship and propeller geometries, it is necessary to check the solution accuracy and study the issues related to mesh independency and then, to verify the accuracy of the results after ensuring their independence from the meshing size. A very important issue of numerical solutions is to validate the obtained results by comparing them with the experimental, numerical, or semi-analytical results.

4.1. Mesh generation analysis

Mesh size and mesh number are important parameters in the numerical analyses; when meshes increase, the computational time increases too and the existing hardware fails to conduct the analyses. Since finer meshes experience increased computational time and cost and larger ones cause computational errors, their size and number should be selected such that the analyses may have the least error and the existing hardware can perform the calculations. Meshes on the ship hull are considered to be much finer than those on

other areas, because the physical phenomena affect it considerably and a steady and high-quality free surface is produced. In this study, modeling of the propeller performance is done based on different meshing for which the thrust coefficient is a comparison factor.

In this study, three types of unstructured meshes were used to calculate the values of thrust, torque, and flow field around the propeller. In this method, a trimmed mesh with the surface growth rate of 1.3 and fast volume growth rate was used. Therefore, the results were obtained using a smaller number of meshes. For grid refinement, the convergence analysis method was employed for the results of mesh independence. The outcome was obtained from four mesh sizes (coarse, medium, fine, and finer) for the propeller.

Based on the Grid Convergence Index method (GCI) proposed by Celik et al. in 2008 [48], the mesh generation analysis was validated. In this method, the apparent orders (p) and $q(p)$ are defined using Eqs. (15) and (16) as follows:

$$p = \frac{1}{\ln(r_{21})} |\ln |\varepsilon_{32}/\varepsilon_{21}| + q(p)|, \quad (15)$$

$$q(p) = \ln \left(\frac{r_{21}^p - s}{r_{32}^p - s} \right), \quad (16)$$

where s is calculated by $s = 1 \cdot \text{sign}(\varepsilon_{32}/\varepsilon_{21})$.

Here, the grid refinement factors for four different meshes, i.e., (1) finer, (2) fine, (3) medium, and (4) coarse, are $r_{21} = h_2/h_1$, $r_{32} = h_3/h_2$, and $r_{43} = h_4/h_3$ (h_i is the basic mesh size). Moreover, for the intended parameter of φ (in the current study K_T), $\varepsilon_{i+1,i}$ is calculated by $\varepsilon_{21} = \varphi_2 - \varphi_1$, $\varepsilon_{32} = \varphi_3 - \varphi_2$, and $\varepsilon_{43} = \varphi_4 - \varphi_3$. In this case, the extrapolated value is defined as Eq. (17):

$$\varphi_{\text{ext}}^{21} = \frac{r_{21}^p \varphi_1 - \varphi_2}{r_{21}^p - 1}. \quad (17)$$

Finally, the relative approximate error (Eq. (18)), extrapolated relative error (Eq. (19)), and fine-grid convergence index (Eq. (20)) were defined as follows:

$$e_a^{21} = \left| \frac{\varphi_1 - \varphi_2}{\varphi_1} \right|, \quad (18)$$

$$\varphi_{\text{ext}}^{21} = \left| \frac{\varphi_{\text{ext}}^{12} - \varphi_1}{\varphi_{\text{ext}}^{12}} \right|, \quad (19)$$

$$GCI_{\text{fine}}^{21} = \frac{1.25 e_a^{21}}{r_{21}^p - 1}. \quad (20)$$

As shown in Table 7, the error rate is very low given that the mesh number is 1.1e6. Thus, this mesh number will be enough for the propeller calculations. In Table 8, the values of these parameters are computed

Table 7. Mesh independency and mesh size effect.

Number of mesh (N)	K_T	The percentage error rate of thrust compared to the previous case	Basic mesh size (m)	Mesh size increase coefficient
750,000	0.153548792	—	0.022	—
800,000	0.152624435	0.65%	0.016	1.062
1,100,000	0.151853246	0.65%	0.012	1.27
1,410,000	0.151264583	0.38%	0.011	1.21

Table 8. Discretization error for propeller thrust (T) based on grid convergence method.

N_1 (finer)	1,410,000	N_3 (medium)	800,000
N_2 (fine)	1,100,000	N_4 (coarse)	750,000
h_1	0.011	h_3	0.016
h_2	0.012	h_4	0.022
r_{21}	1.09	r_{32}	1.33
r_{43}	1.375	φ_1	0.151264583
φ_2	0.151853246	φ_3	0.152624435
φ_4	0.153548792	ε_{21}	0.000588663
ε_{32}	0.000771189	ε_{43}	0.000924357
q	-1.389653346	p	12.991455817
$\varphi_{\text{ext}}^{21}$	0.151746354	e_a^{21}	0.389161156%
e_{ext}^{21}	0.236572241%	GCI_{fine}^{21}	0.2357337073%

Table 9. Comparison of the open-water characteristics of the DTMB4119 propeller (cubical domain).

J	K_T (Num)	K_T (Exp)	$10K_Q$ (Num)	$10K_Q$ (Exp)	η (Num)	η (Exp)
0.5	0.301	0.281	0.495	0.463	0.484	0.483
0.7	0.218	0.207	0.389	0.363	0.624	0.635
0.833	0.16	0.155	0.301	0.28	0.704	0.734
0.9	0.125	0.123	0.263	0.243	0.681	0.725
1.1	0.037	0.037	0.122	0.112	0.537	0.578
Ave. error (%)			3.49%	7.18%		3.97%

for the considered variable of K_T . As shown in Table 8, N_i is the total number of cells; the thrust coefficient is calculated; and the maximum uncertainty is obtained as follows: $GCI_{\text{fine}}^{21} = 0.2357337073\%$.

The selected time step is calculated such that it can rotate between 0.5 and 2 degrees in each step according to the recommendations made in International Towing Tank Conference (ITTC) [49]. Here, the time step for the propeller is 0.0005, which allows the propeller to rotate at 1.9 degrees.

4.2. Validation of the propeller results

The open-water characteristics of the propeller of DTMB4119 are compared with the experimental data [50,51] in two computational domains (cubical and cylindrical domains), as shown in Tables 9 and 10. It

should be noted that the numerical model used is the same as the experimental model. In these tables, J , K_T , K_Q , and η are the advance coefficient, thrust coefficient, torque coefficient, and efficiency of the propeller, respectively. These parameters are defined as follows:

$$K_T = \frac{T}{\rho n^2 D^4}, \quad K_Q = \frac{Q}{\rho n^2 D^5}, \quad (21)$$

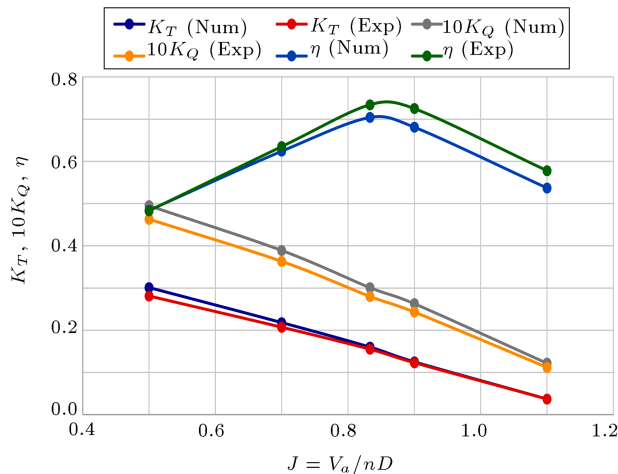
$$\eta = \frac{J K_T}{2\pi K_Q}, \quad J = \frac{V_A}{nD}, \quad (22)$$

where n , D , T , and Q are rotational speed, diameter, thrust, and torque of the propeller, respectively. In Eq. (22), V_A is the advance velocity.

Tables 9 and 10 compare the open-water characteristics of the DTMB4119 propeller in the cubical

Table 10. Comparison of the open-water characteristics of the DTMB4119 propeller (cylindrical domain).

J	K_T (Num)	K_T (Exp)	$10K_Q$ (Num)	$10K_Q$ (Exp)	η (Num)	η (Exp)
0.5	0.308	0.281	0.515	0.463	0.483	0.483
0.7	0.214	0.207	0.389	0.363	0.635	0.635
0.833	0.159	0.155	0.305	0.28	0.734	0.734
0.9	0.124	0.123	0.263	0.243	0.725	0.725
1.1	0.039	0.037	0.121	0.112	0.578	0.578
Ave. error (%)			4.1%		8%	4.28%

**Figure 13.** Comparison of the open-water characteristics of the DTMB4119 propeller (cubical domain).

and cylindrical domains, respectively. The average relative errors of the thrust and torque coefficients and efficiency in the cylindrical domain are 4.1%, 8%, and 4.28%, respectively. The average relative errors of the thrust and torque coefficients and efficiency in the cubical domain are 3.49%, 7.18%, and 3.97%, respectively. Thus, the results indicate that the cubical domain functions relatively better than the cylindrical domain. This domain is generalized to the propeller performance in the wake field including WED (duct and stator). Figure 13 shows the comparison of the open-water characteristics of the DTMB4119 propeller in the cubical domain. At the design speed ($J = 0.833$), the results of the thrust and torque coefficients are in good agreement with the experimental value.

4.3. Wake field prediction

When the ship is moving, the wake flow behind the ship appears to be complicated flow which one can characterize it as unsteady, non-uniform, and rotational due to boundary layer, shape of ship hull, and other factors. Each ship has a typical wake field. To predict the wake field behind the ship, the ship hull should be modeled in the computational domain. The velocity field at the propeller position can be determined. The velocities behind the ship can be predicted using the STAR-CCM+ software. By obtaining the advance velocity behind the KCS ship, the predicted wake factor (w) is

Table 11. Predicted values of wake field behind the KCS.

V_S (kts)	V_M (m/s)	Fn	w
16.83	1.524	0.18	0.278
21.59	1.955	0.23	0.278
23.56	2.134	0.25	0.277
24.00	2.196	0.26	0.275
28.03	2.539	0.30	0.229
30.29	2.743	0.32	0.232

calculated by $w = 1 - V_A/V_S$. Table 11 presents the predicted values of the wake factor at different model speeds. In this table, Fn , V_S , and V_M are Froude number, ship speed, and model speed, respectively. The predicted values of wake factors are found to be around 0.22 ~ 0.28 in which the model speed is changed from 1.524 ($Fn = 0.18$) to 2.743 m/s ($Fn = 0.32$). All numerical results are between the ranges simulated for the wake factor values for KCS. To be specific, they were in between the range $0.25 < w < 0.28$ [52]. As an example, Figure 14 shows the axial and cross-flow velocity contour behind the ship at a model speed of 2.134 m/s ($Fn = 0.25$). The wake factor at this speed is 0.277 and advance velocity is obtained at 1.542 m/s.

4.4. Propeller performance under the wake field

After predicting the wake field, applying it to the solution domain, and checking the propeller performance, the wake field is defined in the solution domain as the input flow. Since the wake field was recorded in the previous section at a point before water entered the propeller, it seems that the propeller is located behind the ship in this simulation and its performance is investigated in the presence of the ship hull and its resulting flow. The numerical results of propeller performance in the wake field are shown in Table 12. As given in the reference site [53], the service speed for the KCS takes 24 knots and with a scale model of 31.599, the advance velocity is 2.196 m/s. As shown in this table, the thrust and torque coefficients decrease and efficiency increases with an increase in the model speed. The efficiency of the ship model at a service

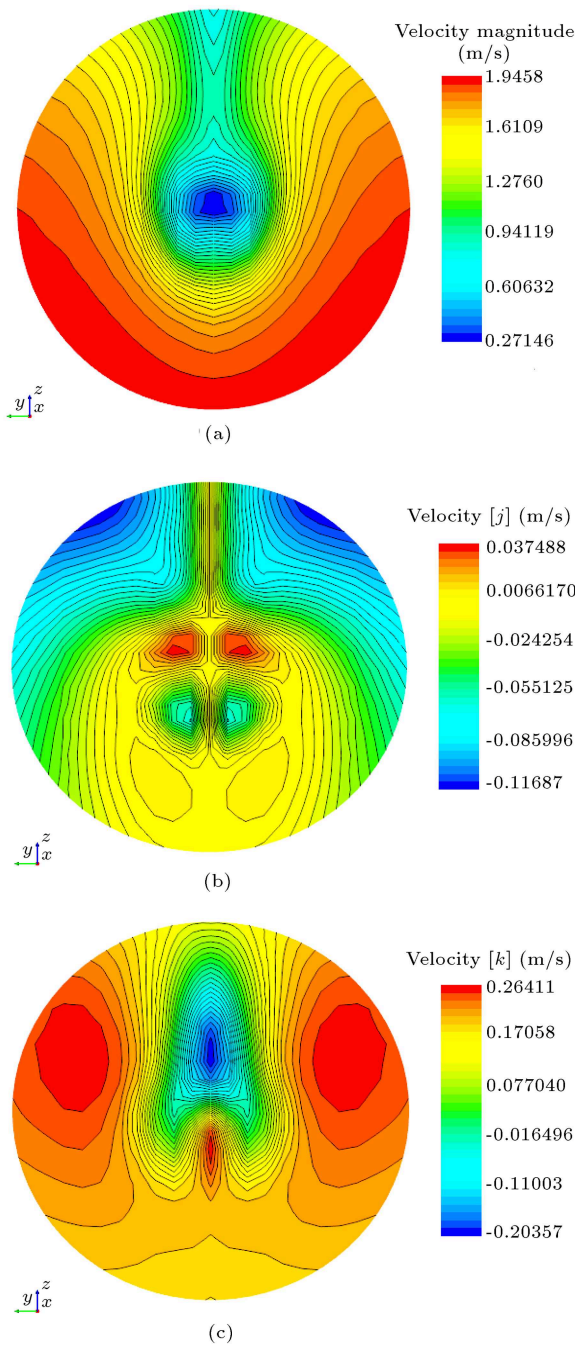


Figure 14. Axial and cross-flow velocity contours behind the ship at the model speed of 2.134 m/s ($F_n = 0.25$): (a) Axial velocity, (b) along the y -axis, and (c) along the z -axis.

speed of 2.196 m/s is 0.489, which seems to be low for this type of DTMB4119 propeller.

4.5. Symmetric and asymmetric ducts

The need to reduce fuel consumption and improve the environmental conditions led to the design of the desired duct and stator to the ship, adapted from similar installed cases in the industry. In the present paper, a duct with NACA4415 section and two types of stators

Table 12. Propeller performance in the wake field.

V_M (m/s)	w	V_A (m/s)	J	K_T	$10K_Q$	η
1.524	0.278	1.1	0.36	0.351	0.566	0.355
2.134	0.277	1.542	0.506	0.277	0.465	0.477
2.196	0.275	1.592	0.522	0.266	0.453	0.489
2.539	0.235	1.940	0.63	0.212	0.380	0.560
2.743	0.232	2.105	0.69	0.186	0.345	0.593



Figure 15. Overview of the symmetrical duct.

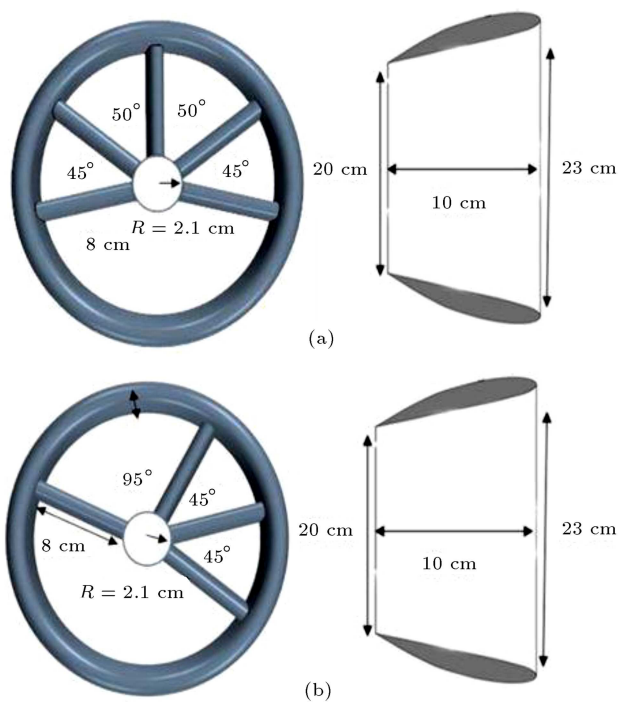
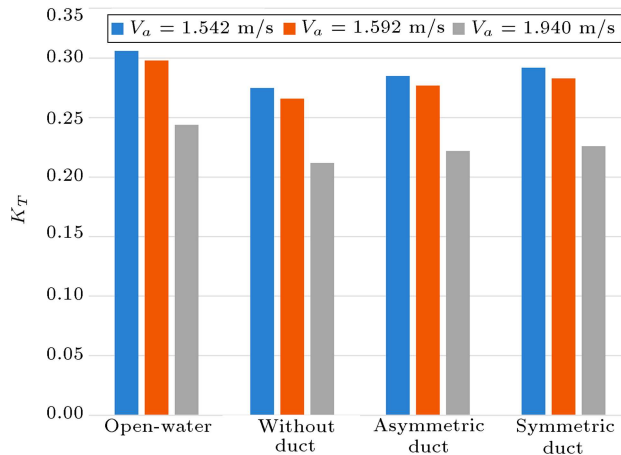
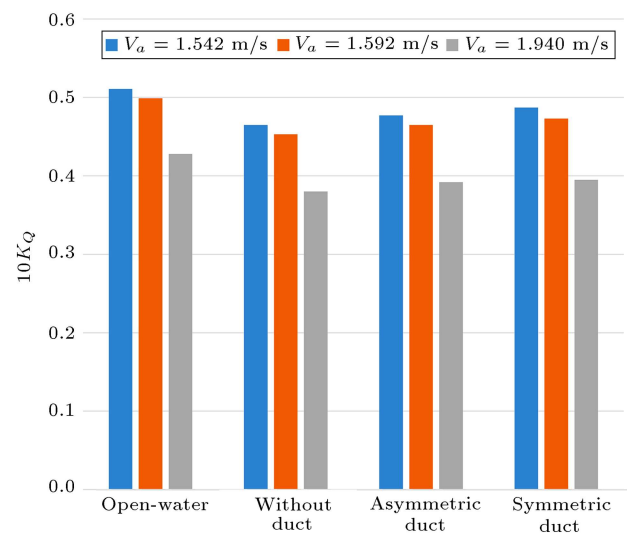


Figure 16. (a) Symmetric duct. (b) Asymmetric duct.

(symmetrical and asymmetrical) is selected. Figure 15 shows an overview of the duct and symmetrical duct mounted at the stern of the ship. Figure 16 shows two types of ducts and stators, which are symmetrical and asymmetrical, respectively, and their effects on the propeller performance are shown. The duct has NACA4415 section type and the stator is NACA0012 section type. The symmetric type has 5 stators placed inside the duct in symmetry to the vertical axis, while

Table 13. Propeller performance in four cases (open-water, without duct, symmetrical duct, and asymmetrical duct).

Behind the ship										
Asymmetric duct		Symmetric duct		Without duct		Open-water		Velocities		
$10K_Q$	K_T	$10K_Q$	K_T	$10K_Q$	K_T	$10K_Q$	K_T	V_A (m/s)	w	V_M (m/s)
0.477	0.285	0.487	0.292	0.465	0.275	0.511	0.306	1.542	0.277	2.134
0.465	0.277	0.473	0.283	0.453	0.266	0.499	0.298	1.592	0.275	2.196
0.392	0.222	0.395	0.226	0.380	0.212	0.428	0.244	1.940	0.229	2.539

**Figure 17.** Comparison of the thrust coefficient under different conditions (open-water, without duct, symmetrical duct, and asymmetrical duct) at three advance velocities.**Figure 18.** Comparison of the torque coefficient under different conditions (open-water, without duct, symmetrical duct, and asymmetrical duct) at three advance velocities.

the asymmetric type has 4 stators, 3 of which are arranged on the right side and one on the left side.

4.6. Hydrodynamic effect

As is evident, the duct provides a condition where the flow is in equilibrium with the propeller, which, in turn, improves the axial velocity. Here, the thrust and torque are presented in Table 13 in four cases (open-water, without duct, symmetrical duct, and asymmetrical duct) and three velocities. Since the advance velocity in open water is greater than that in wake flow, the thrust and torque coefficients are larger than those behind the ship. On the other hand, three cases associated with behind the ship (without duct, symmetric duct, and asymmetric duct) show that the thrust and torque for the symmetric duct are of larger values than the two other cases (asymmetric duct and without duct). To ensure better display, these data are shown in Figures 17 and 18. Based on the results, the gain of the symmetric duct is 6.57%, while the gain of the asymmetric duct is 4.8%.

5. Conclusions

This research studied the Wake Equalizing Duct (WED) and stator mounted in front of the DTMB4119 propeller behind the KRISO Container Ship (KCS).

The purpose of this paper was to determine the hydrodynamic performance of the DTMB4119 propeller by installing new ducts and stators. It appears that one author has previously explored this particular type of propeller combined with the stator and duct. To validate the present numerical results, the available experimental data were used for the propeller under the open-water condition and resistance coefficient of the KCS. Two computational domains of the cubical and cylindrical were used. Thrust and torque coefficients of the propeller were determined at different advance coefficients. Then, the propeller was investigated under the wake flow of the KCS. After predicting the wake behind the ship, two types of ducts (symmetrical and asymmetrical) were mounted in front of the propeller. The following conclusions are drawn from the findings of this study:

- At the model speed of 2.196 m/s (as a service speed of the KCS), the resistance coefficient pointed to the good agreement between the present numerical result and experimental value;
- For propeller open-water calculations, two computational domains of the cubical and cylindrical were

used. It was concluded that the cubical domain caused less error in the numerical solution than the cylindrical domain. The average relative errors for the thrust and torque coefficients and efficiency were 3.49%, 7.18%, and 3.97% in the cubical domain, respectively;

- The efficiency was reduced when the propeller operated behind the ship compared to the open-water condition. At the service speed of 2.196 m/s, the efficiencies were 0.497 and 0.489 in the open-water condition and behind the ship, respectively;
- Improvement rates for the propeller performance after mounting the asymmetric and symmetric ducts were 4.8% and 6.57%, respectively.

Nomenclature

\bar{B}_i	Average body force
\bar{P}_i	Average fluid hydrostatic pressure
\bar{u}_i	Average velocity
\bar{u}'_i	Average oscillating velocity
$\bar{\rho}'$	Average oscillating density
h_i	Basic mesh sizes
B_i	Body force
C_t	Resistance coefficient
K_Q	Torque coefficient
K_T	Thrust coefficient
N_i	The total number of cells
P_i	Instantaneous hydrostatic pressure
P_κ	Turbulence production rate
Re_L	Reynolds number based on the ship's length
V_M	Model speed
V_S	Ship speed
e_a^{ij}	Relative approximate error
e_{ext}^{ij}	Extrapolated relative error
r_{ij}	Grid refinement factor
u_i	Instantaneous velocity
u'_i	Oscillating velocity
μ_t	Turbulent viscosity
$\bar{\rho}$	Average density
σ_k	Prandtl number
σ_ε	Turbulent Schmidt number
$\varphi_{\text{ext}}^{ij}$	Extrapolated value
Δy	First wall thickness of the boundary layer
μ	Fluid viscosity
B	Breath of KCS model

B	Production buoyancy loss
D	Depth of ship
Fn	Froude number
G	Turbulence kinetic energy
GCI	Grid Convergence Index
J	Advance coefficient
L	Ship length
LPP	Length between Perpendiculars
LWL	Length of Waterline
P	Hydrostatic pressure
T	Draft of ship
U	Velocity vector
w	Wake factor
k	Kinetic energy
ε	Rate of dissipation of turbulent kinetic energy
η	Efficiency
ρ	Density vector
$\rho u'_i u'_j$	Reynolds's tension
φ	Intended parameter

References

1. Ziarati, R., Bhuiyan, Z., De Melo, G., et al. "MariEMS train the trainee (MariTTT) courses on energy efficient ship operation", Technical Report (2017).
2. Choi, Y.B. "2008.11 DSME ship energy saving devices: Hydrodynamics R&D team", In The House of Wisdom and Innovation, Technical report (2008).
3. Skipsreyyen Company "The green solution below the waterline", <https://www.skipsreyyen.no/article/the-green-solution-below-the-waterline> (Accessed 15 February 2018).
4. Wärtsilä Encyclopedia of Marine Technology. Power-Saving Devices, <https://www.wartsila.com/encyclopedia/term/power-saving-devices> (Accessed 14 August 2019).
5. Carlton, J., *Marine Propellers and Propulsion*, 3th Edn., Butterworth Heinemann, J.S. (2012).
6. Park, S., Oh, G., Rhee, S.H., et al. "Full scale wake prediction of an energy saving device by using computational fluid dynamics", *Ocean Engineering*, **101**, pp. 254–263 (2015).
7. Kim, J.H., Choi, J.E., Choi, B.J., et al. "Development of energy-saving devices for a full slow-speed ship through improving propulsion performance", *International Journal of Naval Architecture and Ocean Engineering*, **7**(2), pp. 390–398 (2015).
8. Mizzi, K., Demirel, Y.K., Banks, C., et al. "Design optimisation of propeller boss cap fins for enhanced propeller performance", *Applied Ocean Research*, **62**, pp. 210–222 (2017).

9. Go, J.S., Yoon, H.S., and Jung, J.H. “Effects of a duct before a propeller on propulsion performance”, *Ocean Engineering*, **136**, pp. 54–66 (2017).
10. Gaggero, S., Villa, D., Tani, G., et al. “Design of ducted propeller nozzles through a RANSE-based optimization approach”, *Ocean Engineering*, **145**, pp. 444–463 (2017).
11. Chang, X., Sun, S., Zhi, Y., et al. “Investigation of the effects of a fan-shaped Mewis duct before a propeller on propulsion performance”, *Journal of Marine Science and Technology*, **24**(1), pp. 46–59 (2019).
12. Andersen, S.V. “Numerical treatment of the design-analysis problem of ship propellers using vortex lattice methods”, PhD Thesis, DTU, Lyngby, Denmark (1988).
13. Baltazar, J., and Falcao de Campos, J.A.C. “On the modelling of the flow in ducted propellers with a panel method”, In *Proceedings of the 1st International Symposium on Marine Propulsors*, **9**, pp. 1–15 (2009).
14. Cai, H.P., Su, Y.M., Li, X., et al. “Using the surface panel method to predict the steady performance of ducted propellers”, *Journal of Marine Science and Application*, **8**(4), pp. 275–280 (2009).
15. Baltazar, J., Falcão de Campos, J.A.C., and Bosschers, J. “Open-water thrust and torque predictions of a ducted propeller system with a panel method”, *International Journal of Rotating Machinery*, **2012** (2012).
16. Lee, D., Jang, B.S., and Kim, H. “Development of procedure for structural safety assessment of energy saving device subjected to nonlinear hydrodynamic load”, *Ocean Engineering*, **116**, pp. 165–183 (2016).
17. Gaggero, S. “Design of PBCF energy saving devices using optimization strategies: A step towards a complete viscous design approach”, *Ocean Engineering*, **159**, pp. 517–538 (2018).
18. Nowruzi, H. and Najafi, A. “An experimental and CFD study on the effects of different pre-swirl ducts on propulsion performance of series 60 ship”, *Ocean Engineering*, **173**, pp. 491–509 (2019).
19. Tacar, Z., Sasaki, N., Atlar, M., et al. “An investigation into effects of gate rudder[®] system on ship performance as a novel energy-saving and maneuvering device”, *Ocean Engineering*, **218**, p. 108250 (2020).
20. Obwogi, E.O., Shen, H.L., and Su, Y.M. “The design and energy saving effect prediction of rudder-bulb-fin device based on CFD and model test”, *Applied Ocean Research*, **114**, p. 102814 (2021).
21. Ghasemi, H. “The effect of wake flow and skew angle on the ship propeller performance”, *Scientia Iranica*, **16**(2), pp. 149–158 (2009).
22. Ghassemi, H., Mardan, A., and Ardeshir, A. “Numerical analysis of hub effect on hydrodynamic performance of propellers with inclusion of PBCF to equalize the induced velocity”, *Polish Maritime Research*, **19**(2(73)), pp. 17–24 (2012).
23. Shamsi, R. and Ghassemi, H. “Time-accurate analysis of the viscous flow around puller podded drive using sliding mesh method”, *Journal of Fluids Engineering*, **137**(1), pp. 1–9 (2015).
24. Majdfar, S., Ghassemi, H., Forouzan, H., et al. “Hydrodynamic prediction of the ducted propeller by CFD solver”, *Journal of Marine Science and Technology*, **25**(3) (2017).
25. Esmailian, E., Ghassemi, H., and Zakerdoost, H. “Systematic probabilistic design methodology for simultaneously optimizing the ship hull-propeller system”, *International Journal of Naval Architecture and Ocean Engineering*, **9**(3), pp. 246–255 (2017).
26. Mahmoodi, K., Ghassemi, H., and Nowruzi, H. “Obtaining mathematical functions of the propeller thrust and torque coefficients fluctuations at non-uniform wake flow including geometry effects”, *Mechanics & Industry*, **19**(2), p. 205 (2018).
27. Zakerdoost, H. and Ghassemi, H. “Hydrodynamic optimization of ship’s hull-propeller system under multiple operating conditions using MOEA/D”, *Journal of Marine Science and Technology*, **26**(2), pp. 419–431 (2020).
28. Martinas, G. “Cavitation of a propeller and influence of a wake equalizing duct”, *TransNav: International Journal on Marine Navigation and Safety of Sea Transportation*, **9**(2), pp. 235–241 (2015).
29. Ok, J.P. and Hamburg-Harburg, TU “Power savings by wake equalizing ducts?”, *Ship Technology Research*, **52**(1), pp. 34–51 (2005).
30. Korkut, E. “A case study for the effect of a flow improvement device (a partial wake equalizing duct) on ship powering characteristics”, *Ocean Engineering*, **33**(2), pp. 205–218 (2006).
31. Çelik, F. “A numerical study for effectiveness of a wake equalizing duct”, *Ocean Engineering*, **34**(16), pp. 2138–2145 (2007).
32. Heinke, H.-J. and Hellwig-Rieck, K. “Investigation of scale effects on ships with a wake equalizing duct or with vortex generator fins”, In *Second International Symposium on Marine Propulsors*, Hamburg, Germany (2011).
33. Streckwall, H. and Xing-Kaeding, Y. “On the working principle of pre-swirl stators and on their application benefit and design targets”, *International Shipbuilding Progress*, **63**(3–4), pp. 87–107 (2017).
34. Lee, K.J., Lee, H.D., and Choi, S.H. “A design and validation study of a non-axisymmetric preswirl stator”, *Ocean Engineering*, **189**, p. 106365 (2019).
35. Han, C. “Optimization and design research on marine pre-swirl stator-propeller by CFD”, Master thesis, Harbin Engineering University, Harbin, China (2019).
36. Lee, K.S., Kim, M.C., Shin, Y.J., et al. “Design of asymmetric pre-swirl stator for KVLCC2 considering angle of attack in non-uniform flow fields of the stern”, *Journal of the Society of Naval Architects of Korea*, **56**(4), pp. 352–360 (2019).

37. Furcas, F., Vernengo, G., Villa, D., et al. “Design of wake equalizing ducts using RANSE-based SBDO”, *Applied Ocean Research*, **97**, p. 102087 (2020).
38. Nadery, A. and Ghassemi, H. “Numerical investigation of the hydrodynamic performance of the propeller behind the ship with and without WED”, *Polish Maritime Research* (2020).
39. Koushan, K., Krasilnikov, V., Nataletti, M., et al. “Experimental and numerical study of pre-swirl stators PSS”, *Journal of Marine Science and Engineering*, **8**(1), p. 47 (2020).
40. Nadery, A., Ghassemi, H., and Nowruzi, H. “Enhancement of the ship propeller hydrodynamic performance by different energy-saving devices mounted at the upstream zone”, *Journal of the Brazilian Society of Mechanical Sciences and Engineering*, **43**(10), pp. 1–25 (2021).
41. Nadery, A., Ghassemi, H., and Chybowski, L. “The effect of the PSS configuration on the hydrodynamic performance of the KP505 propeller behind the KCS”, *Ocean Engineering*, **234**, p. 109310 (2021).
42. Su, Y.M., Lin, J.F., Zhao, D.G., et al. “Influence of a pre-swirl stator and rudder bulb system on the propulsion performance of a large-scale ship model”, *Ocean Engineering*, **218**, p. 108189 (2020).
43. Guo, C.Y., Xu, P., Han, Y., et al. “Working mechanism of pre-swirl stator based on stereoscopic particle image velocimetry”, *Ocean Engineering*, **236**, p. 109442 (2021).
44. Qin, D., Huang, Q., Pan, G., et al. “Effect of the duct and the pre-swirl stator on the wake dynamics of a pre-swirl pumpjet propulsor”, *Ocean Engineering*, **237**, p. 109620 (2021).
45. Mikkelsen, H., Shao, Y., and Walther, J.H. “Numerical study of nominal wake fields of a container ship in oblique regular waves”, *Applied Ocean Research*, p. 102968 (2022).
46. Carrica, P.M., Fu, H., and Stern, F. “Computations of self-propulsion free to sink and trim and of motions in head waves of the KRISO Container Ship (KCS) model”, *Applied Ocean Research*, **33**(4), pp. 309–320 (2011).
47. Feng, D., Ye, B., Zhang, Z., et al. “Numerical simulation of the ship resistance of KCS in different water depths for model-scale and full-scale”, *Journal of Marine Science and Engineering*, **8**(10), p. 745 (2020).
48. Celik, I.B., Ghia, U., Roache, P.J., et al. “Procedure for estimation and reporting of uncertainty due to discretization in CFD applications”, *Journal of Fluids Engineering-Transactions of the ASME*, **130**(1), pp. 1–4 (2008).
49. ITTC Proceedings “Practical guidelines for ship CFD applications ITTC - Recommended procedures and guidelines”, *Section 7.5-03-02-03, International Towing Tank Conference* (2014).
50. Sezen, S., Doğrul, A., and Şakir, B.A.L. “An empirical approach for propeller tip vortex cavitation noise”, *Sigma Journal of Engineering and Natural Sciences*, **36**(4), pp. 1127–1139 (2018).
51. Boumediene, K. and Belhenniche, S.E. “Numerical analysis of the turbulent flow around DTMB 4119 marine propeller”, *Int. J. Mech. Aerosp. Ind. Mechatron. Manuf. Eng.*, **10**, pp. 347–351 (2016).
52. Kinaci, O.K., Gokce, M.K., Alkan, A.D., et al. “On self-propulsion assessment of marine vehicles”, *Brodogradnja: Teorija i Praksa Brodogradnje i Pomorske Tehnike*, **69**(4), pp. 29–51 (2018).
53. Workshop on verification and validation of ship maneuvering simulation methods (SIMMAN 2008), Copenhagen, Denmark, 14-16 April 2008, MOERI Container Ship (KCS), <http://www.simman2008.dk/KCS/kcs-geometry.htm> (2012, accessed 10 March 2019).

Biography

Saman Rezaei received his MSs degree in Naval Architecture from Amirkabir University of Technology (Tehran Polytechnic). He is currently a PhD student of Maritime Engineering at the Department of Mechanical Engineering at Sharif University of Technology. He has researched on Marine Energy Device (ESD) and his current research interests include Marine Autonomous Surface Ship (MASS) collision avoidance methods base on COLREG.

Milad Bamdadinejad received the BSc degree in Civil-Surveying Engineering from the Department of Geodesy and Geomatics Engineering at Tafresh University in 2014 and the MSc degree in Coastal Engineering from the Department of Maritime Engineering at Amirkabir University of Technology (Tehran Polytechnic) in 2018. His research interests include application of remote sensing and GIS in coastal engineering, marine renewable energy, and coastal sediment transport modeling.

Hassan Ghassemi is a Professor at Amirkabir University of Technology (AUT). His research interests include ocean renewable energy, marine propulsor design, dynamics of offshore structures, high-speed craft, and hydrodynamic numerical methods such as BEM and CFD.